Available online at www.sciencedirect.com
SCIENCE DIRECT®
Journal of Power Sources 146 (2005) 457–463
JOURNAL OF POWER SOURCES
www.elsevier.com/locate/jpowsour

Changes of electro-deposited Sn–Ni alloy thin film for lithium ion battery anodes during charge discharge cycling

H. Mukaibo [a], T. Momma [a,b], T. Osaka [a,*]

[a] *Graduate School of Science and Engineering, Waseda University, 3-4-1, Okubo, Shinjyuku-ku, Tokyo 169-8555, Japan*
[b] *CREST, Japan Science and Technology Agency, Japan*

Available online 27 April 2005

Abstract

We have reported in our past work that electrodeposited Sn–Ni alloy with different composition show considerably different performance as anode materials for Li-ion batteries, and the performance was remarkably well (ca. 650 mAh g^{-1} at 70th cycle) when the composition was controlled to $Sn_{62}Ni_{38}$. In this work, structural changes during charge discharge cycling of Sn–Ni alloy with different composition were investigated to evaluate their differences in the cycle performance. From the XRD result, Ni_3Sn_4 phase was the main phase seen in $Sn_{62}Ni_{38}$, and its reversible reactivity with Li was confirmed. We suggest that this is the key phase for its high capacity and lengthened cycle life. From $Sn_{54}Ni_{46}$, which showed low capacity, only a metastable phase close to the structure of SnNi was confirmed. The results from $Sn_{84}Ni_{16}$ indicated the presence of pure Sn and Sn rich metastable phase would lead to relatively fast electrode degradation.

Keywords: Sn–Ni alloy; Electrodeposition; Anode

1. Introduction

Li-ion batteries possess the highest energy density among the practical batteries, and the development of its anode material is considered as one of the breakthroughs to meet the demands for power sources with higher performance for portable electronic devices.

Presently, carbon is used as the anode material for Li-ion batteries, which is now showing a capacity close to its theoretical value of 372 mAh g^{-1}. As one of the researches for the development of Li-ion batteries, Fuji Film Company filed a patent for Sn oxide in 1994 as a novel anode material that could replaced the conventional carbonaceous material with higher capacity [1]. However, this material showed two fatal defects, high initial irreversible capacity and shorter life, compared to that of carbon. For these reasons, it could not be applied to practical use. Courtney and Dahn have reported that, in the case of Sn oxide anode, Sn is the key to the high discharge capacity and Li_2O acts as a matrix that helps to lengthen the cycle life of the electrode [2]. Without the matrix, the electrode would suffer more rapid degradation [3]. Since then, researches have focused on the selection of adequate matrix that eases the electrode stress, which appears during cycling, effectively for longer cycle life.

Elements that are inactive against Li (such as Ni) are assumed to suppress the volume change effectively without much irreversible capacity [3–20]. We have confirmed in our past work that the Sn–Ni alloy thin film prepared from electrodeposition has the potential to perform as the anode of Li-ion battery, and that the composition of $Sn_{62}Ni_{38}$ leads to a high discharge capacity of ca. 650 mAh g^{-1} at about the 70th cycle (Fig. 1) [21].

In the present study, we focused on the differences in morphology and structure of the Sn–Ni alloy thin film with different composition during charge discharge cycling. Ex situ XRD and SEM were applied to the films in different charged–discharged state to evaluate the correlation between the electrode structure, surface morphology and the cycle performance.

* Corresponding author. Tel.: +81 3 5286 3202; fax: +81 3 3205 2074.
E-mail address: osakatet@waseda.jp (T. Osaka).

0378-7753/$ – see front matter © 2005 Elsevier B.V. All rights reserved.
doi:10.1016/j.jpowsour.2005.03.043

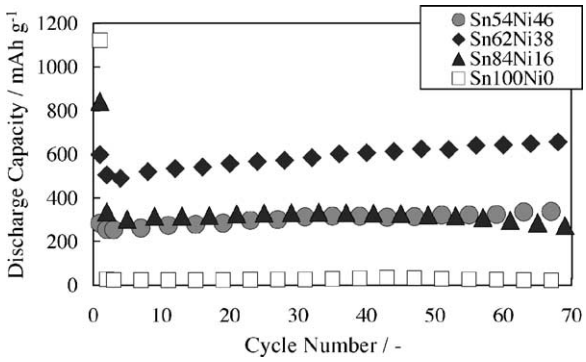

Fig. 1. Cycle performance of electrodeposited Sn_xNi_y thin films reproduced from Ref. [21].

2. Experimental

The Sn–Ni thin films with different composition were prepared by electrodeposition on Cu sheet from potassium pyrophosphate baths at 50 °C according to the procedure reported [22]. Each film was deposited for 5 min with the current density of 5 mA cm^{-2}. The compositions of the films were determined by inductively coupled plasma-atomic emission spectroscopy (Thermo Electron K.K., IRIS-AP). The anodes were cycled in conventional glass cells, with two pieces of Li foil as counter and reference electrodes and the organic electrolyte was 1 M $LiClO_4$/ethylene carbonate (EC) + propylene carbonate (PC) (1:1 vol.%). The electrochemical cells were assembled and sealed under dry Ar atmosphere (dew point was kept under −100 °C).

The galvanostatic cycling was performed using a charge–discharge equipment (Hokuto Denko, HJR-1010mSM8) in the potential range of 0.01–1.20 V versus Li/Li^+. Both charge and discharge were carried out at the current density of 250 mA g^{-1} of Sn–Ni alloy. The electrodes were rested for 10 min between charge and discharge. The cycling for structural and morphological examination was processed in a constant current–constant potential (CC–CP) mode. When in this mode during charging, the electrodes are charged in constant current until 0.01 V versus Li/Li^+ and then kept at this potential until 4 h have passed since the beginning of the charging step. Conversely, during the discharging step, the electrodes are discharged in constant current until 1.20 V versus Li/Li^+ and then kept at this potential until 4 h have passed in total. X-ray diffraction was performed on Rigaku RAD-IC using Cu Kα radiation. XRD conditions of voltage and current measurements were 40 kV and 20 mA, respectively, and the scan rate was set at 2° min^{-1}. Morphology of the film was imaged using a scanning electron microscope (HITACHI, S2500CX). Grain size, cross sectional morphology and the electron diffraction patterns of $Sn_{62}Ni_{38}$ were evaluated using transmission electron microscope (HITACHI, H-9000NAR), with samples prepared using FIB equipment (Seiko Instruments Inc., SMI-8300II). The acceleration voltage was 300 kV and the diameter of the analyzing beam for electron diffraction pattern was 2 nm.

3. Results and discussion

We have indicated that Sn–Ni alloy shows different anodic features with different compositions from our previous work, as shown in Fig. 1 [21]. Under the assumption that all Sn reacts with Li to form $Li_{4.4}Sn$, the theoretical capacity of $Sn_{54}Ni_{46}$, $Sn_{62}Ni_{38}$, and $Sn_{84}Ni_{16}$ would be 700, 763, and 909 mAh g^{-1}, respectively. Nevertheless, when they were cycled, $Sn_{54}Ni_{46}$ and $Sn_{84}Ni_{16}$ showed a relatively low discharge capacity of ca. 300 and 272 mAh g^{-1} after 70 cycles. Under the same condition, $Sn_{62}Ni_{38}$ showed the largest discharge capacity of 654 mAh g^{-1}. Another interesting feature of these samples is that they show increase in capacity with cycling after first several cycles. $Sn_{62}Ni_{38}$ showed the biggest increase in 70 cycles (166 mAh g^{-1}). $Sn_{54}Ni_{46}$ also increased about 100 mAh g^{-1} of its capacity in 70 cycles, but the capacity of $Sn_{84}Ni_{16}$ started to decrease in about 35 cycles after 30 mAh g^{-1} increase of its capacity. To evaluate these phenomena, structural and morphological changes with cycling (repeated Li^+ insertion and extraction) were investigated by XRD and SEM. Since the results of $Sn_{92}Ni_8$ reported in our previous work were similar to that of $Sn_{84}Ni_{16}$, this paper will only discuss the results of the latter case.

Fig. 2 illustrates the structure and surface morphology of $Sn_{54}Ni_{46}$, $Sn_{62}Ni_{38}$ and $Sn_{84}Ni_{16}$ before cycling. The peak assignments of the XRD are based on the results of Watanabe et al. who carried out a detailed study on the structure of electroplated Sn–Ni films [23]. Metastable phases are phases that do not appear in the equilibrium phase diagram; formed due to the electrodeposition process. The metastable phase M1 is a NiSn phase with a composition ratio of almost 50:50, and the metastable phase M2 is a phase where Ni is melted into pure Sn crystal lattice. M1 phase is the main phase confirmed from the XRD of $Sn_{54}Ni_{46}$ and not identified in $Sn_{62}Ni_{38}$ or $Sn_{84}Ni_{16}$. For $Sn_{62}Ni_{38}$, Ni_3Sn_4 phase is the only identified phase. Calculation assuming that all the Ni atom within $Sn_{62}Ni_{38}$ is forming Ni_3Sn_4 alloy with Sn, leaves at least 19 at.% Sn in excess. Nevertheless, presence of distinct pure Sn phase could not be distinguished from Fig. 2. Consulting that the peaks attributed to Ni_3Sn_4 in our results are slightly shifted from those indicated in the JCPDS data, these Sn may exist melted within the Ni_3Sn_4 lattice, or exist as a nano-crystalline or an amorphous phase in the film. The XRD peaks of $Sn_{84}Ni_{16}$ are assigned to Ni_3Sn_4, M2 and pure Sn phases. Peaks at 34.5°, 35°, 42.2° and 46.7° could not be identified. From SEM observation, the majority particles size of $Sn_{54}Ni_{46}$, $Sn_{62}Ni_{38}$ and $Sn_{84}Ni_{16}$ was 20–24, 25–29, and 40–44 nm, respectively, and films with higher Sn content lead to rougher, more granular surface.

Fig. 3 shows the results of the XRD patterns and SEM images after the first charging (Li insertion). Upon charging, the peak attributed to M1 phase of $Sn_{54}Ni_{46}$ at 30.3°

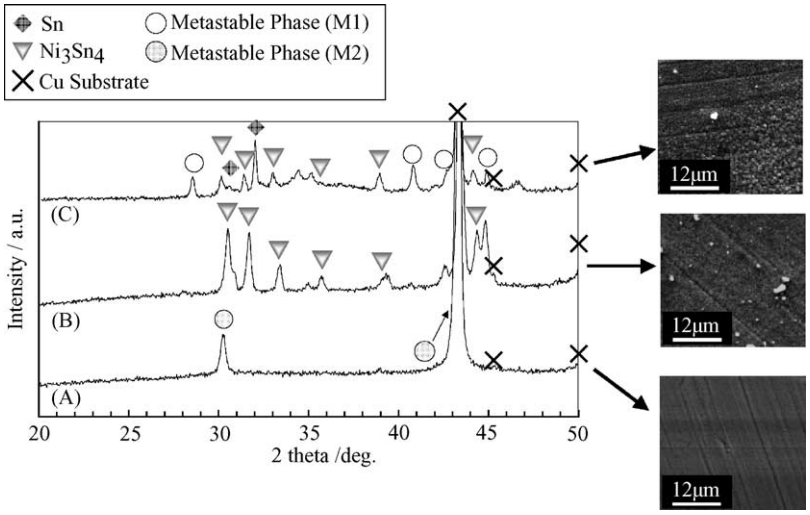

Fig. 2. XRD patterns and SEM images of (A) $Sn_{54}Ni_{46}$, (B) $Sn_{62}Ni_{38}$, and (C) $Sn_{84}Ni_{16}$ before cycling.

decreases its intensity. This suggests that part of the phase reacted with Li^+, resulting in a state of nano-crystalline or amorphous phase that could not be detected by the XRD. It should also be noted that no peaks assigned to Li–Sn alloy phase were confirmed at this charged state. This indicates that no XRD-detectable Li–Sn binary alloy phases were formed by the reaction of Sn with Li^+. On the contrary, $Sn_{62}Ni_{38}$ and $Sn_{84}Ni_{16}$ showed new peaks indicating the presence of Li–Sn alloys. As it is well known, there are several types of Li–Sn alloys with different composition [24–26]. However, the results here show them as two broad peaks, and since many peaks of various Li–Sn composition is overlapped in this range, it was not possible to attribute them to a certain Li–Sn phase. This indicates that lithiation reaction of Sn had taken place during charging in $Sn_{62}Ni_{38}$ and $Sn_{84}Ni_{16}$ thin films. Simultaneously, most of the peaks due to Ni_3Sn_4, M2 and Sn phase became unidentifiable. Peaks attributed to pure Ni were not identified. This will be discussed further with the results shown in Fig. 4. The SEM images of each sample after Li^+ insertion showed a bumpier surface compared to those images before cycling (Fig. 2).

After the first discharge process where Li^+ was extracted from the sample (Fig. 4), the XRD patterns suggest a partial recovery of the electrode structure. For $Sn_{54}Ni_{46}$, the peak intensity of the metastable phase at 30.3° grows higher again, indicating that the reaction between the M1 phase and Li^+ is reversible. The peak is also slightly broader than it was before cycling (Fig. 2) suggesting the decrease in the crystal size. In the case of $Sn_{62}Ni_{38}$, although all the peaks attributed to Ni_3Sn_4 in Fig. 2 were confirmed again, their peak intensity had become relatively weaker. From the XRD pattern of $Sn_{84}Ni_{16}$, only the peak at 45° was identified for M2 phase. Recovery of all the peaks of Ni_3Sn_4 and Sn were confirmed, but their peak intensity was different from Fig. 2 without regularity. Specifically, compared with the peak intensities of Fig. 2, the peaks at 30.3° (Ni_3Sn_4), 30.7° (Sn), 31.5° (Ni_3Sn_4)

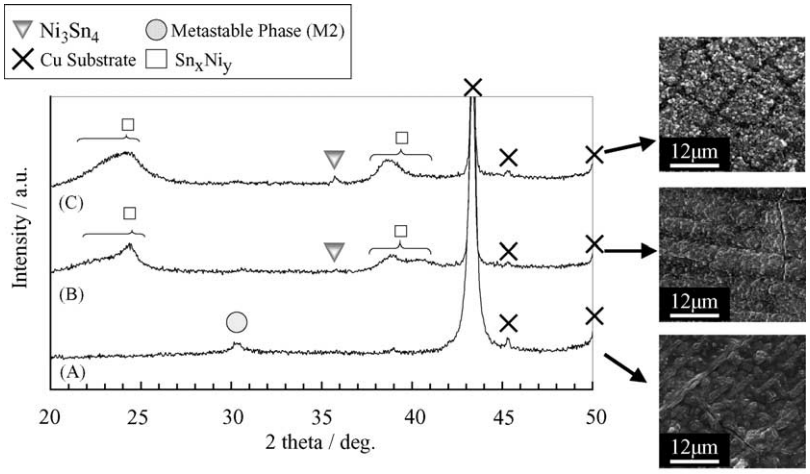

Fig. 3. XRD patterns and SEM images of (A) $Sn_{54}Ni_{46}$, (B) $Sn_{62}Ni_{38}$, and (C) $Sn_{84}Ni_{16}$ after initial charging. Charged until 0.01 V vs. Li/Li^+ at the constant current density of 250 mA g^{-1} in 1 M $LiClO_4$/EC + PC (1:1 vol.%) organic electrolyte.

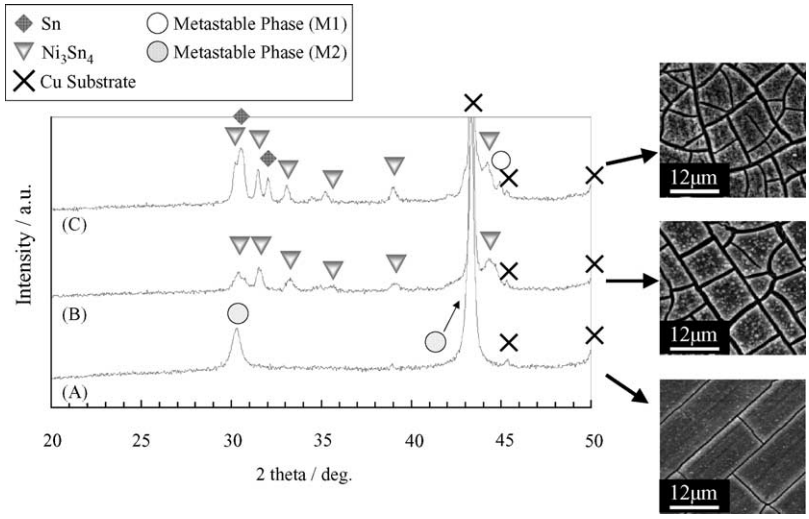

Fig. 4. XRD patterns and SEM images of (A) $Sn_{54}Ni_{46}$, (B) $Sn_{62}Ni_{38}$, and (C) $Sn_{84}Ni_{16}$ after first discharge. Cycled in the potential range of 0.01–1.20 V vs. Li/Li^+ at the constant current density of 250 mA g^{-1} in 1 M $LiClO_4$/EC + PC (1:1 vol.%) organic electrolyte.

and 44.2° (Ni_3Sn_4) showed increased intensity, while the peak at 33.1° (Ni_3Sn_4) and 45.0° (Sn) showed almost the same intensity, and peaks at 32.0° (Sn), 35.8° (Ni_3Sn_4) and 39.0° (Ni_3Sn_4) showed decreased intensity. The peaks attributed to Li–Sn alloy phases were no longer detectable for both $Sn_{62}Ni_{38}$ and $Sn_{84}Ni_{16}$. Assuming from the fact that the Ni–Sn alloy phase has recovered in both $Sn_{62}Ni_{38}$ and $Sn_{84}Ni_{16}$ with Li^+ extraction, Ni may have existed within the film in the charged state (Fig. 3) as nano-crystalline or amorphous phase; hence their phases could not be identified in XRD results. From the SEM images, formation of surface cracks with Li^+ extraction was confirmed. Relatively, the cracks after discharging are smaller for $Sn_{54}Ni_{46}$. This may be indicating that the reaction of M1 phase and Li^+ shows smaller volume change compared to the reaction between Ni_3Sn_4 and Li^+. This may be considered to be consistent with the smaller amount of Li insertion (lower discharge capacity) indicated in Fig. 1. Also, these cracks confirmed on the electrode surface can be expected to lower the diffusion resistance of Li^+ into the inner electrode. This generation of cracks may be one of the reasons for the rise in the capacity with cycling seen in the cycle performance of each electrodeposited Sn–Ni alloy anode (Fig. 1 [21]).

Fig. 5 shows the XRD results and SEM images of each sample after the 10th discharge (Li extraction). For $Sn_{54}Ni_{46}$ and $Sn_{62}Ni_{38}$, no more formation of new phases or disappearance of existing phases can be confirmed compared with the result for the sample after first discharge (Fig. 4), while both samples showed lower peak intensity. Especially for $Sn_{62}Ni_{38}$, it may be noted that the XRD result does not indicate aggregation of pure Sn phase with cycling as reported for Sn oxide materials [27]. For $Sn_{84}Ni_{16}$, all the peaks attributed

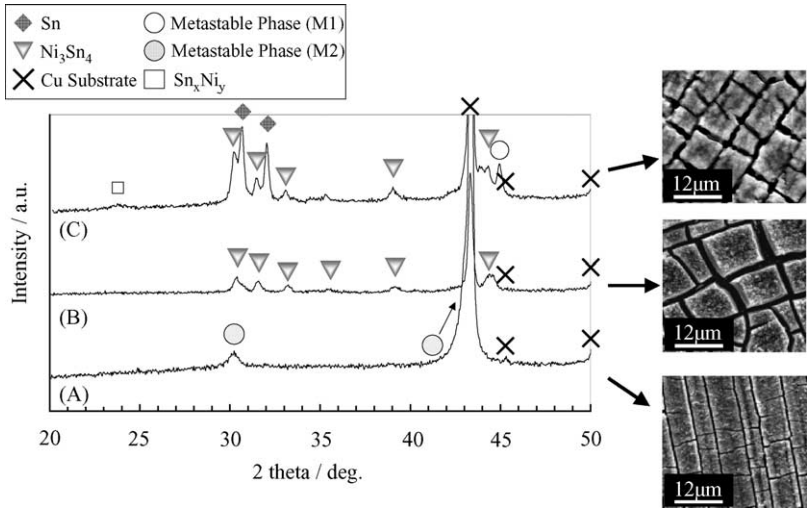

Fig. 5. XRD patterns and SEM images of (A) $Sn_{54}Ni_{46}$, (B) $Sn_{62}Ni_{38}$, and (C) $Sn_{84}Ni_{16}$ after 10th discharge. Cycled in the potential range of 0.01–1.20 V vs. Li/Li^+ at the constant current density of 250 mA g^{-1} in 1 M $LiClO_4$/EC + PC (1:1 vol.%) organic electrolyte.

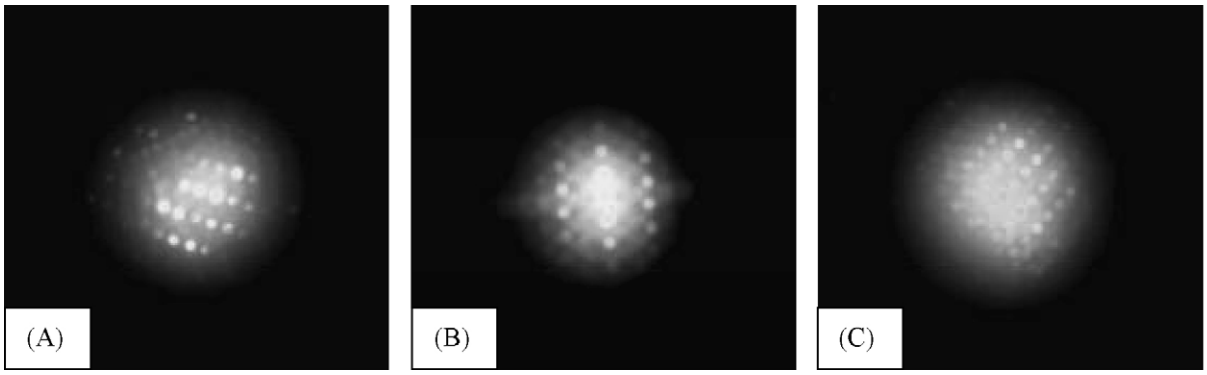

Fig. 6. μ-Electron diffraction pattern of $Sn_{62}Ni_{38}$ (A) as deposited, (B) after the first charge, and (C) after the first discharge. Cycled in the potential range of 0.01–1.20 V vs. Li/Li^+ at the constant current density of 250 mA g^{-1} in 1 M $LiClO_4$/EC + PC (1:1 vol.%) organic electrolyte.

to Sn showed increase in its intensity that may be indicating the aggregation of Sn phase with cycling. Furthermore, this sample showed small peak that was attributed to Li–Sn alloy phase at the lower degree (around 25°). This suggests that with repeated cycling, some Li gets trapped within the Li–Sn alloy, unable to dealloy during the discharge process. The SEM images show the similar cracked surface morphology as Fig. 4.

The change of the electrode crystallinitiy with cycling was also evaluated using μ-ED (Fig. 6). Clear Laue patterns can be seen from the as-deposited image and from the 1st discharge image, indicating its crystallinity. But after the first charge, broad halo can be identified, suggesting that the Li insertion has a significant effect on lowering the crystallinity of the electrode structure in the nanometer scale.

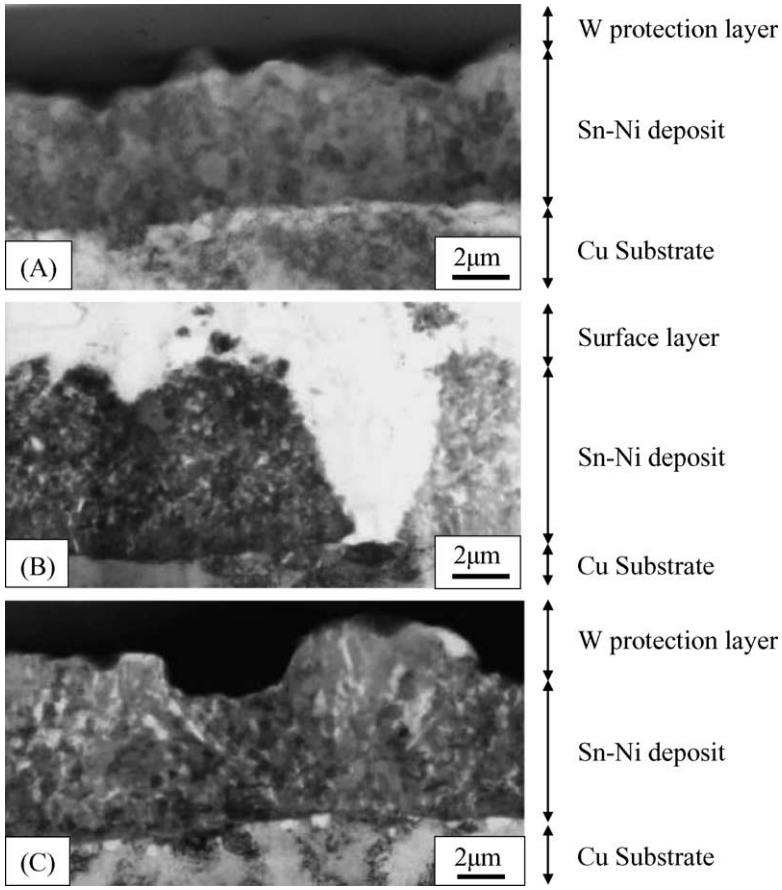

Fig. 7. TEM images of the $Sn_{62}Ni_{38}$ (A) as deposited, (B) after the first charge, and (C) after the first discharge. The $Sn_{62}Ni_{38}$ electrode was cycled in the potential range of 0.01–1.20 V vs. Li/Li^+ at the constant current density of 250 mA g^{-1} in 1 M $LiClO_4$/EC + PC (1:1 vol.%) organic electrolyte.

Table 1
Summary of the TEM results

State of sample	Film thickness (μm)	Crystal particle size (μm)	Film state	Surface film
Before cycling	0.6	0.05–0.13	Dense	Not confirmed
After first charge	1.25	0.01–0.13	Porous	Confirmed
After first discharge	0.75	0.01–0.18	Porous	Not confirmed

Overall, the obtained results suggest that a reaction mechanism of Sn–Ni alloys is different to the ones considered for the Sn oxide anodes [2]. With the Li^+ insertion during the charge process, Sn atoms segregate from the Sn–Ni alloy structure and alloys with Li to form the Li–Sn alloy phase. This reaction should be reversible. With discharge, the Li^+ is extracted from the Li–Sn alloy phase, and the dealloyed Sn atom gets absorbed into the Ni matrix again forming the Sn–Ni alloy phase.

Considering this reaction mechanism with the gained results on the cycle performance and structural changes of the electrodes, it may be suggested that the structure of $Sn_{54}Ni_{46}$ was unable to free the Sn from the metastable Sn–Ni alloy crystal to allow its full alloying with Li. This could also be supported by the fact that the initial discharge capacity was 597 mAh g^{-1} for $Sn_{62}Ni_{38}$ and 841 mAh g^{-1} for $Sn_{84}Ni_{16}$ but 334 mAh g^{-1} for $Sn_{54}Ni_{46}$. In the case of $Sn_{84}Ni_{16}$, pure Sn phases were observed which clearly did not alloy with Ni, hence leading to the large capacity drop after the second cycle. The rechargeable capacity also begins to drop from the 35th cycle indicating its relatively rapid degradation compared to $Sn_{54}Ni_{46}$ and $Sn_{62}Ni_{38}$ (Fig. 1 [21]).

It was indicated that the structure that allows Li and Sn, Sn and Ni to reversibly alloy/dealloy is the key to gain high-capacity long-life anode materials. Ni_3Sn_4 phase may have been able to realize such reversible reactions, hence resulting in the high capacity of $Sn_{62}Ni_{38}$.

To obtain further information on the changes induced by cycling, cross-sectional TEM pictures were taken on $Sn_{62}Ni_{38}$ (Fig. 7), which showed the highest performance as Li-ion battery anodes during galvanostatic cycling test [21]. The film thickness of $Sn_{62}Ni_{38}$ before cycling was ca. 0.6 μm, and the crystal particle size was 0.05–0.13 μm. The film thickness and crystal particle size varied largely upon cycling, and formation of cracks and pores were seen with cycling. The results are summarized in Table 1. With the first charging discharging process, the dense film became porous, and the thickness expanded. The surface layer seen on the film upon charging disappeared with discharging. This may indicate the growth of Li oxides during the procedure to prepare TEM samples by exposure to the air. Or it may indicate some decomposition of the organic electrolyte during charging. Decrease in the crystal size of the film was also confirmed with cycling. This may be due to the reaction where Li comes into the Ni_3Sn_4 phase to generate Ni-rich and Li–Sn alloy phases, and to the converse reaction where Li goes out from the Li–Sn alloy and Ni-rich phases and generate Ni_3Sn_4 phases. This reversible reaction could be contributing to the good anode property of $Sn_{62}Ni_{38}$.

4. Conclusion

A reaction mechanism of Sn–Ni alloys that is different to the ones considered for the Sn oxide anodes [2] was suggested from the Sn–Ni alloys with different composition ($Sn_{54}Ni_{46}$, $Sn_{62}Ni_{38}$, and $Sn_{84}Ni_{16}$) that show different anode properties. With the Li^+ insertion during the charge process, Sn atoms segregate from the Sn–Ni alloy structure and alloys with Li to form the Li–Sn alloy phase. This reaction should be reversible, and with discharge, the Li^+ is extracted from the Li–Sn alloy phase, and the dealloyed Sn atom gets absorbed into the Ni matrix again forming the Sn–Ni alloy phase.

It was suggested that the structure of $Sn_{54}Ni_{46}$ was unable to free the Sn from the metastable Sn–Ni alloy crystal to allow its full alloying with Li. For $Sn_{84}Ni_{16}$, pure Sn phases were observed which clearly did not alloy with Ni, hence leading to the large capacity drop after the second cycle. It was indicated that the structure that allows Li and Sn, Sn and Ni to reversibly alloy/dealloy is the key to gain high-capacity long-life anode materials. Ni_3Sn_4 phase may realize such reversible reactions, and $Sn_{62}Ni_{38}$, which was mainly composed of this Ni_3Sn_4 structure, results in high capacity.

It was also indicated that the lithiation procedure has the effect of lowering the crystallinity of the electrode. Formation of surface cracks with cycling was also confirmed with cycling. This generation of cracks may be one of the reasons for the rise in the capacity with cycling seen in the cycle performance of each electrodeposited Sn–Ni alloy anodes.

Acknowledgements

This work is supported in part by a Grant-in-Aid for Scientific Research (A), 15205024, and Center of Excellence (COE) Research “Molecular Nano-Engineering from the Ministry of Education, Culture, Sports, Science and Technology”, and conducted at the 21st Century COE Program “The center for Practical Nano-Chemistry”. Hitomi Mukaibo acknowledges a research fellowship from the Japan Society for the Promotion of Science.

References

[1] Fuji Photo Film Co. Ltd., European Patent 0,651,450, A1 (1995).

[2] I.A. Courtney, J.R. Dahn, J. Electrochem. Soc. 144 (1997) 2045.
[3] N. Tamura, R. Ohshita, M. Fujimoto, S. Fujitani, M. Kamino, I. Yonezu, J. Power Sources 107 (2002) 48.
[4] O. Mao, R.L. Turner, I.A. Courtney, B.D. Fredericksen, M.I. Buckett, L.J. Krause, J.R. Dahn, Electrochem. Solid-State Lett. 2 (1999) 3.
[5] O. Mao, R.A. Dunlap, J.R. Dahn, J. Electrochem. Soc. 146 (1999) 405.
[6] O. Mao, R.A. Dunlap, J.R. Dahn, J. Electrochem. Soc. 146 (1999) 414.
[7] O. Mao, R.A. Dunlap, J.R. Dahn, J. Electrochem. Soc. 146 (1999) 423.
[8] D. Larcher, L.Y. Beaulieu, O. Mao, A.E. George, J.R. Dahn, J. Electrochem. Soc. 147 (2000) 1703.
[9] K.D. Kepler, J.T. Vaughey, M.M. Thackeray, Electrochem. Solid-State Lett. 2 (1999) 307.
[10] D. Larcher, L.Y. Beaulieu, D.D. MacNeil, J.R. Dahn, J. Electrochem. Soc. 147 (2000) 1658.
[11] G.X. Wang, L. Sun, D.H. Bradhurst, S.X. Dou, H.K. Liu, J. Alloys Compd. 299 (2000) L12.
[12] L. Beaulieu, D. Larcher, R.A. Dunlap, J.R. Dahn, J. Alloys Compd. 297 (2000) 122.
[13] G.M. Ehrlich, C. Durand, X. Chen, T.A. Hugener, F. Spiess, S.L. Suib, J. Electrochem. Soc. 147 (2000) 886.
[14] O. Crosnier, T. Brousse, X. Devaux, P. Fragnaud, D.M. Schleich, J. Power Sources 94 (2001) 169.
[15] J. Ahn, Y. Kim, G. Wang, M. Lindsay, H.K. Liu, S. Dou, Mater. Trans. 43 (2002) 63.
[16] O. Crosnier, Doctorate Thesis, University of Nantes, 2001.
[17] H.Y. Lee, S.W. Jang, S.M. Lee, S.J. Lee, H.K. Baik, J. Power Sources 112 (2002) 8.
[18] J.-H. Ahn, G.X. Wang, J. Yao, H.K. Liu, S.X. Dou, J. Power Sources 119–121 (2003) 45.
[19] S. Yamate, J. Maruta, T. Murata, H. Yasuda, M. Yamachi, Proceedings of the 44th Battery Symposium in Japan, 2002 (abstract no. 3B04).
[20] Y.-L. Kim, H.-Y. Lee, S.-W. Jang, S.-J. Lee, H.-K. Baik, Y.-S. Yoon, Y.-S. Park, S.-M. Lee, Solid State Ionics 160 (2003) 235.
[21] H. Mukaibo, T. Sumi, T. Yokoshima, T. Momma, T. Osaka, Electrochem. Solid-State Lett. 6 (2003) A218.
[22] A. Ito, H. Enomoto, J. Met. Fin. Soc. Jpn. 36 (1985) 466.
[23] T. Watanabe, T. Hirose, K. Arai, M. Chikazawa, J. Jpn. Inst. Met. 63 (1999) 496.
[24] C.J. Wen, R.A. Huggins, J. Electrochem. Soc. 128 (1981) 1181.
[25] J. Chouvin, J. Olivier-Fourcade, J.C. Jumas, B. Simon, O. Godiveau, Chem. Phys. Lett. 308 (1999) 413.
[26] M. Winter, J.O. Besenhard, Electrochim. Acta 45 (1999) 31.
[27] I.A. Courtney, W.R. McKinnon, J.R. Dahn, J. Electrochem. Soc. 146 (1999) 59.